Geophysical Journal International

Geophys. J. Int. (2013) **193,** 1119–1132
Advance Access publication 2013 March 19

doi: 10.1093/gji/ggt060

Geomechanics of fracture caging in wellbores

Ruud Weijermars,[1,2] Xi Zhang[3] and Dan Schultz-Ela[4]

[1]*Department of Geoscience & Engineering, Delft University of Technology, Stevinweg* 1, *Delft* 2628CN, *the Netherlands. E-mail: R.Weijermars@TUDelft.nl*
[2]*Alboran Energy Strategy Consultants, Delft, the Netherlands*
[3]*CSIRO Earth Science and Resource Engineering, Ian Wark Laboratory, Bayview Avenue, Clayton* 3168, *Victoria, Australia*
[4]*Colorado, Department of Computer Science, Mathematics & Statistics, Colorado Mesa University,* 1100 *North Avenue, Grand Junction,* CO 81501, *USA*

Accepted 2013 February 11. Received 2013 February 9; in original form 2012 July 14

SUMMARY

This study highlights the occurrence of so-called 'fracture cages' around underbalanced wellbores, where fractures cannot propagate outwards due to unfavourable principal stress orientations. The existence of such cages is demonstrated here by independent analytical and numerical methods. We explain the fracture caging mechanism and pinpoint the physical parameters and conditions for its control. This new insight has great practical relevance for the effectiveness and safety of drilling operations in general, and hydraulic fracturing in particular. Fracture caging runaway poses a hazard for drilling operations in overpressured formations. Recognition of the fracture caging mechanism also opens up new opportunities for controlled engineering of its effects by the manipulation of the Frac number in wells in order to bring more precision in the fracking process of tight formations.

Key words: Geomechanics; Equations of state; Fracture and flow.

1 INTRODUCTION

This study introduces an improved theoretical framework for wellbore stress manipulation in well control and hydraulic fracture engineering. Carefully selected stress trajectory patterns are visualized and characterized by a non-dimensional number (see later) using static stress function solutions (Weijermars 2011; Weijermars *et al.* 2012) and compared to dynamic numerical solutions using a fully coupled hydraulic fracture model (Zhang *et al.* 2011a,b). The matching theoretical results (Fig. 1) confirm the possibility that fracture cages may occur in so-called underbalanced boreholes, which directs fractures to curl around wellbores.

The occurrence of spalling (or exfoliation) by tension failure near underpressured circular holes has been reported before in laboratory experiments (Vardoukalis *et al.* 1988; Roest *et al.* 1989). Slabbing is a similar process reported from deep tunnels and shafts (Durrheim *et al.* 1995; Ortlepp 2001), where spontaneous rockburst is the most visible expression of tension stress normal to the walls of manmade excavations. Similarly, drilling engineers have long known that empty drill holes tend to collapse due to the pressure of the wall rock, which may give rise to splintery cavings. This is exactly the reason why heavy bentonite mud is circulated down drillholes (Ahmed & Meehan 2012) to keep the pressure on the inside of the wellbore high enough—so-called overbalancing—to prevent it from collapsing inwards.

Traditionally, the stress patterns around wellbores have been modelled using dimensional equations of Ernst Gustav Kirsch (1898), a 19th century German engineer who described the elastic stress around a hole in an infinite plate under unidirectional tension. The Kirsch equations have been adapted since several times (Malvern 1969; Zoback 2007; Zang & Stephansson 2009). The analytical stress function solutions derived in non-dimensional form (Weijermars 2011) capture the intricate interaction of hydraulically induced stresses with the geological far-field stress and takes into account the effect of any unbalanced formation pressures. We introduce the non-dimensional Frac number (for definition see Box 1) to produce universal stress trajectory solutions and describe the physical conditions under which fracture cages may occur.

We emphasize that the term 'fracture cage' (for definition see Box 1) introduced by us (Weijermars *et al.* 2012), is different from the term 'stress cage'. The latter term has been used to describe the rise in tangential stresses around a wellbore due to dilation and propping of early fractures (Alberty & McLean 2004; Wang *et al.* 2008; Tovar & Bhat 2011). Obviously, the two mechanisms relate but fracture cages and stress cages each require their own specific analysis. Fracture cages are complementary to stress cages, which is why we maintain a link in the terminology. The occurrence of fracture cages is highlighted here in detail for the first time. Analytical stress solutions predict the conditions leading to fracture cages and the phenomenon was confirmed in a numerical model (see later). We outline the two models—static analytical and dynamic numerical—and highlight the practical implications for prudent well management.

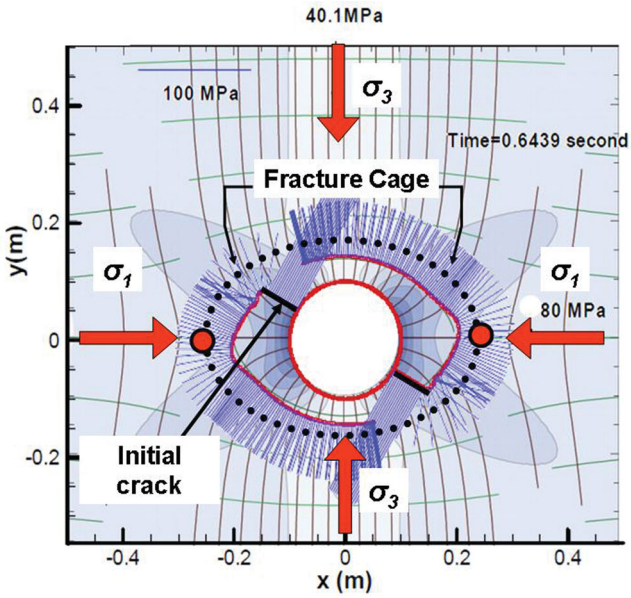

Figure 1. Fracture cage predicted by analytical stress trajectory solutions superposed on numerical solution. The initial crack near the wellbore (black solid lines, 0.64 times borehole radius) in this fracture growth simulation can not escape from the fracture cage formed by the deviatoric stress trajectories around the wellbore. Red curvilinears show propagating fractures curl around the wellbore and stay trapped inside the fracture cage (black dots). Red arrows show far field total stresses (σ_1 and σ_3) and red dots are isotropic points.

BOX 1. Definition of fracture caging terms.

Frac number: Non-dimensional ratio of the net pressure on wellbore in the nominator and the absolute value of the principal far field deviatoric compressive stress in the denominator, valid for a specific borehole section where these physical units are constant.

Fracture cage: Confined space around borehole where the principal deviatoric compressional stress follows concentric rings so that any radial fracture emanating from the wellbore into the fracture cage space will remain trapped inside and rotate into the direction of the concentric tension rings (normal to the tension stress, which is radial inside the fracture cage). A negative Frac number is a prerequisite for the occurrence of a fracture cage.

Fracture caging: Formation of concentric tension fractures and shear joint breakouts inside a fracture cage space due to underbalanced drilling relative to an overpressured formation penetrated by the wellbore, which renders the Frac number for that wellbore section negative.

Fracture caging runaway: Progressive widening of wellbore width due to sustained fracture caging as circumferential tension fractures continue to form new and wider fracture cages that collapse inwards while the removal of rock debris by upward flow through the production annulus creates room for further fracture caging as long as the Frac number remains negative and the net pressure large enough to continue collapse of the wellbore section by tension failure and shear joint breakout.

2 SYMBOLS AND SUBSCRIPTS FOR ANALYSIS OF WELLBORE PHYSICS

In our paper, total stress is denoted by σ and deviatoric stress by τ. Deviatoric stresses differ from the total stress in that isotropic stresses (pressure components) cause volumetric deformation in isotropic material and deviatoric stresses cause shape deformation. Although uniform volumetric deformation may give rise to deviatoric stresses, the isotropic stress components in rock do not direct fracture formation, which is why we focus on deviatoric stress in our analysis. The deviatoric stress can be represented in both a tensor and principal form. There are three principal deviatoric stresses τ_1, τ_2 and τ_3 of which—in our analysis—the intermediate stress (τ_2) is assumed to be aligned with the drilling direction and the two other principal stresses are in the transverse direction. The in-plane 'far field' stresses τ_1 and τ_3 will determine the stress trajectory exactly the same as that determined by total stress. There is also no difference in determining the principal stress from far-field deviatoric stresses τ_1 and τ_3, and from total stresses with symbols σ_1 and σ_3, except for an isotropic term. This notation is in compliance with common practice in structural geology literature (Weijermars 1998; Fossen 2010).

We have deliberately chosen the structural geology notation and depart from the traditional approach in drilling engineering, which denotes a maximum total stress in the horizontal plane by σ_H (or $\sigma_{H\,MAX}$) and a minimum by σ_h (or $\sigma_{H\,MIN}$) and a vertical stress by σ_v. We include Tables 1 and 2 to aid comparison and conversion of our symbols, subscripts and sign convention to alternative, traditional approaches. We use the physical effects of principal stresses, that is, compression and tension to fix the subscripts. Henceforth, compressional stresses are in our study consistently denoted by σ_1 and τ_1 in compliance with the prevailing annotation in structural geology and tectonic models. Our notation, using σ_1, σ_2, and σ_3, is arguably more practical when matching our solutions to the natural range of tectonic regimes (Andersonian, amplified with transpressional and transtensional cases) as is elaborated in a related study (Weijermars & Schulz-Ela 2012). The physical meaning of wellbore pressures and stresses is adequately and consistently described by our symbols, subscripts and sign convention.

3 STRESS FUNCTION ANALYSIS

Our analytical description of wellbore stresses uses two stress functions, Φ_1 and Φ_2. The first stress function (Φ_1) specifies all stresses induced by the wellbore net pressure, $\overrightarrow{P}_{NET}$, on the wellbore wall and in the rock volume beyond in a polar (r, θ) reference frame (Fig. 2):

$$\Phi_1(r,\theta) = \overrightarrow{P}_{NET} a^2 \ln r \qquad (1)$$

with radius of the drill hole, a. Eq. (1) excludes any effect of geological far-field stresses, but a second stress function (Φ_2) is introduced to specify the deviatoric stresses around the borehole due to the superposed effects of any far-field stresses

$$\Phi_2(r,\theta) = +(\tau_1/4)r^2 - (\tau_1/2)a^2 \ln(r/a) + [(\tau_1/4)r^2 - (\tau_1/2)a^2 + (\tau_1/4)(a^4/r^2)\cos 2\theta]. \qquad (2)$$

Summation of the two stress functions (eqs 1 and 2) provides a comprehensive stress function (Weijermars 2011), which fully accounts for the deviatoric stresses around a borehole due to the combination of $\overrightarrow{P}_{NET}$ and far-field stress τ_1.

Table 1. Notation used.

Physical quantity	Symbol	Justification and meaning
Total stress	σ	Includes pressure components (when absent, $\sigma = \tau$)
Deviatoric stress	τ	Effective stress, excludes the confining pressure component
Principal total stress	$\sigma_1\ \sigma_2\ \sigma_3$	Invariants for coordinate system used, these are the real physical total stresses independent of tensor orientation
Principal deviatoric stress	$\tau_1\ \tau_2\ \tau_3$	Invariants for coordinate system used, these are the real physical deviatoric stresses independent of tensor orientation
Far field stress Total Deviatoric	 $\sigma_1\ \sigma_2\ \sigma_3$ $\tau_1\ \tau_2\ \tau_3$	'Far field' principal stress values for both total and deviatoric forms
Net pressure on wellbore	$\vec{P}_{\mathrm{NET}}$	Scalar pressures on the wall rock surface of the wellbore induce a normal stress equal to $\vec{P}_{\mathrm{NET}}$ (see Section 5) an sign convention is given in Fig. 4
Compressive stress sign	Positive	Makes compressive stress and confining pressure positive. Extensional stress and expansive pressure is negative.
Largest absolute deviatoric stress	$\lvert\tau_1\rvert$	Concurs with applied geoscientist use of maximum compressive stress as σ_1, even when compressive stress is taken negative as in our study
Frac number	$\vec{P}_{\mathrm{NET}}/\lvert\tau_1\rvert$	Uniquely scales the stress trajectory pattern around the wellbore based on non-dimensional stress function solutions and deviatoric stress contributions of $\vec{P}_{\mathrm{NET}}$ and τ_1

Table 2. Corresponding principal total stresses and σ_{H}, σ_{h} and σ_{V}, depending on tectonic stress regime.

Tectonic setting of basin	Orientation invariant principal stresses		
Principal stress subscripts valid for all cases	σ_1	σ_2	σ_3
Tectonic setting of basin	Conversion to spatially fixed subscripts		
Collision	σ_{H}	σ_{h}	σ_{V}
Extension	σ_{V}	σ_{h}	σ_{H}
Strike slip	σ_{H}	σ_{V}	σ_{h}
Transtension	σ_{V}	σ_{h}	σ_{H}
Transpression	σ_{H}	σ_{h}	σ_{V}

Note: For deviatoric stress conversions, use τ instead of σ for all symbols used in this table.

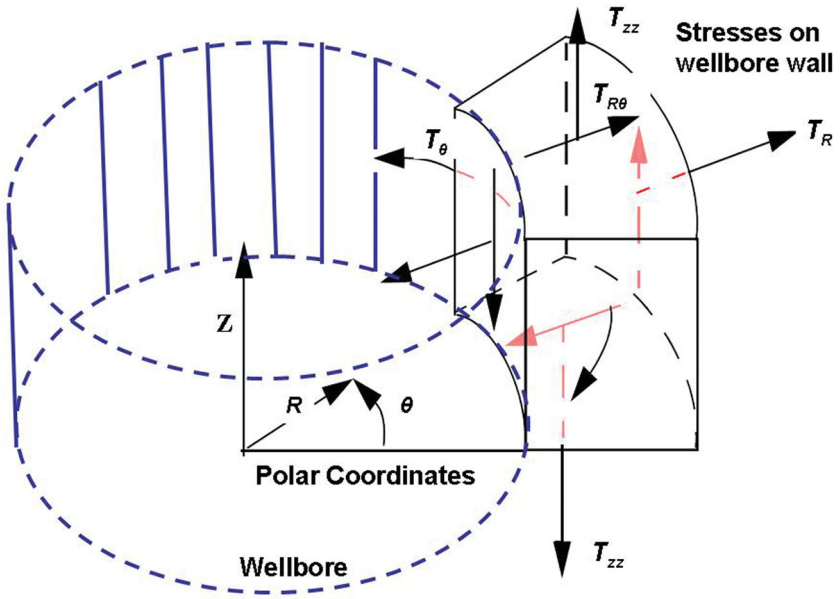

Figure 2. Polar coordinates around wellbore. Reference frame is chosen to be aligned with wellbore so tensor notation retains its most simple form.

The magnitude of the elements of the stress tensor in polar coordinates (R, θ)-space (Fig. 2) is given by (Weijermars 2011)

$$\tau_r = \overrightarrow{P}_{\mathrm{NET}}(a/R)^2 + (\tau_1/2)\left[\left[1-(a/R)^2\right]\right] - \left[\left[1-4(a/R)^2+3(a/R)^4\right]\cos 2\theta\right], \quad (3a)$$

$$\tau_\theta = -\overrightarrow{P}_{\mathrm{NET}}(a/R)^2 + (\tau_1/2)\left[\left[1+(a/R)^2\right]\right] + \left[\left[1+3(a/R)^4\right]\cos 2\theta\right], \quad (3b)$$

$$\tau_{r\theta} = -(\tau_1/2)\left[1-3(a/R)^4+2(a/R)^2\right]\sin 2\theta. \quad (3c)$$

We introduce a non-dimensional scaling parameter coined the Frac number $F = \overrightarrow{P}_{\mathrm{NET}}/|\tau_1|$ and adopt non-dimensional polar coordinate space (R^*, θ) with radial coordinates normalized by the wellbore radius a according to $R^* = R/a$. These scaling operators transform eqs 3(a)–(c) to their non-dimensional form (Weijermars 2011):

$$\tau_r^* = \left(1/R^{*2}\right) + (1/2F)\left[\left[1-\left(1/R^{*2}\right)\right]\right] - \left[\left[1-\left(4/R^{*2}\right)+\left(3/R^{*4}\right)\right]\cos 2\theta\right], \quad (4a)$$

$$\tau_\theta^* = -\left(1/R^{*2}\right)+(1/2F)\left[\left[1+\left(1/R^{*2}\right)\right]+\left[1+\left(3/R^{*4}\right)\right]\cos 2\theta\right], \quad (4b)$$

$$\tau_{r\theta}^* = -\left(1/2F\right)\left[1-\left(3/R^{*4}\right)+\left(2/R^{*2}\right)\right]\sin 2\theta. \quad (4c)$$

The principal stress trajectory pattern in (R^*, θ)-space is now fully determined by the inclination β of a stress trajectory with respect to the wellbore axis (Weijermars 2011):

$$\tan 2\beta = 2\tau_{r\theta}^*/\left(\tau_r^* - \tau_\theta^*\right) \quad (5)$$

with the two conjugate solutions for β separated by $\pi/2$. A continuous solution of eq. (5) outlines the stress trajectories in a spatial plane perpendicular to the wellbore. The static analytical solutions of the wellbore stress patterns have been computed and visualized later in this study using standard software. The stress trajectories are mapped for the continuous range of all possible ratios of $\overrightarrow{P}_{\mathrm{NET}}$ and regional far field stress τ_1, which control the scaling factor, F, in eqs 4(a)–(c) and (5). Our analytical expressions for the magnitude of the stress tensor components (eqs 3a–c) are similar to previous borehole stress solutions (e.g. Zang & Stephansson 2009). We use an uniaxial solution and introduce a practical non-dimensional scaling parameter ($F = \overrightarrow{P}_{\mathrm{NET}}/|\tau_1|$), which allows continuous mapping of the stress trajectories when inserted in the stress function sum $\Phi_1 + \Phi_2$ (see Weijermars 2011).

4 FRAC NUMBER

The advantage of the non-dimensional stress function description of eqs 4(a)–(c) is that all possible stress patterns around a wellbore can be characterized by the single Frac number:

$$F = \overrightarrow{P}_{\mathrm{NET}}/|\tau_1| \quad (6)$$

with wellbore net-pressure, $\overrightarrow{P}_{\mathrm{NET}}$, which induces deviatoric stresses on the wellbore host rock, cf. eq. (1), and τ_1 is the deviatoric compressive stress due to the far-field stress resident in the host rock. The absolute value $|\tau_1|$ is taken to reduce confusion over sign conventions. Mechanical engineers traditionally use a positive sign for tensile stress, and geotechnical engineers often take compressive stress as positive. The relative magnitudes of the 2-D parameters in the Frac number, $\overrightarrow{P}_{\mathrm{NET}}$ and τ_1, fully determine the stress function solutions of eqs 4(a)–(c). The deviatoric far field stress, τ_1, is the non-isotropic far-field stress component, sometimes termed the anisotropic stress, which is naturally present in many hydrocarbon basins. This regime of principal stresses may be classified as extensional, compressional, transtensional or transpressional (Weijermars 1993, 1998; Fossen 2010).

Fig. 3 maps the full range of non-dimensional stress trajectory patterns uniquely identified by the scalar F-number. The upper half of the plot accounts for the overbalanced wellbores and the lower half for underbalanced wellbores. The distinction between the stress trajectory patterns for each of the two regimes is elaborated in the remainder of our study. The key message is that fracture propagation around overbalanced wellbores follows preferential directions oriented differently from those around underbalanced wellbores and the principal stress trajectory patterns help to explain why this is the case. For all patterns, the absolute stress magnitudes can be obtained from eqs 3(a)–(c).

5 NET PRESSURE

The Frac number is critically dependent on $\overrightarrow{P}_{\mathrm{NET}}$ which warrants a more detailed discussion on the physical parameters that control $\overrightarrow{P}_{\mathrm{NET}}$. For all cases summarized in Fig. 3, $\overrightarrow{P}_{\mathrm{NET}}$ represents the effective (net) pressure exerted as a static stress on the wellbore wall (Fig. 4), which is responsible for a deviatoric stress pattern in the host rock of the wellbore described by eq. (1).

Our analytical solution assumes a static wellbore pressure differential on the wellbore (Fig. 5a). Pressure of stationary (non-flowing) fluids always works perpendicular to the solid wellbore contact surface. The force responsible for deviatoric stress is the pressure differential between the mud load in the wellbore and the fluid pressure in the adjacent formation given by:

$$\overrightarrow{P}_{\mathrm{NET}} = \overrightarrow{P_{\mathrm{M}}} + \overrightarrow{P_{\mathrm{F}}} = P_{\mathrm{M}} - P_{\mathrm{F}}, \quad (7)$$

where $\overrightarrow{P_{\mathrm{M}}}$ is the hydraulic force per unit area on the wellbore due the mud load and P_{M} the scalar pressure on the wellbore, $\overrightarrow{P_{\mathrm{F}}}$ is the formation fluid pressure on the wellbore (with opposite sign) and P_{F} the scalar formation pressure. Scalar pressures for both P_{M} and P_{F} involve fluid loads, which therefore are always positive in their respective regions. However, they act as opposing force vectors at either side of the wellbore.

In tight formations the formation fluid pressure cannot directly communicate with the wellbore fluid, as the rocks are in the nano-Darcy permeability regime. Yet our analysis is particularly relevant for nano-Darcy rocks as it predicts stress trajectories for hydraulic fracking (see Section 9.2). For tight, impermeable rocks in the nano-Darcy regime, we expand the definition of formation pressure to account for wellbore tractions due three mechanisms (Fig. 5a):

$$P_{\mathrm{F}} = P_{\mathrm{P}} + P_{\mathrm{L}} + P_{\mathrm{T}}, \quad (8)$$

where P_{P} is the trapped fluid pressure in the formation (commonly due to time-dependent compaction), P_{L} is the lithostatic pressure due to the rock overburden and P_{T} is the isotropic component of the tectonic stress, which for incompressible rock is the mean total tectonic stress $P_{\mathrm{T}} = (\sigma_1 + \sigma_2 + \sigma_3)/3$. $\overrightarrow{P}_{\mathrm{NET}}$ may also vary at depth, depending on the relative magnitude of all four variables P_{M}, P_{P},

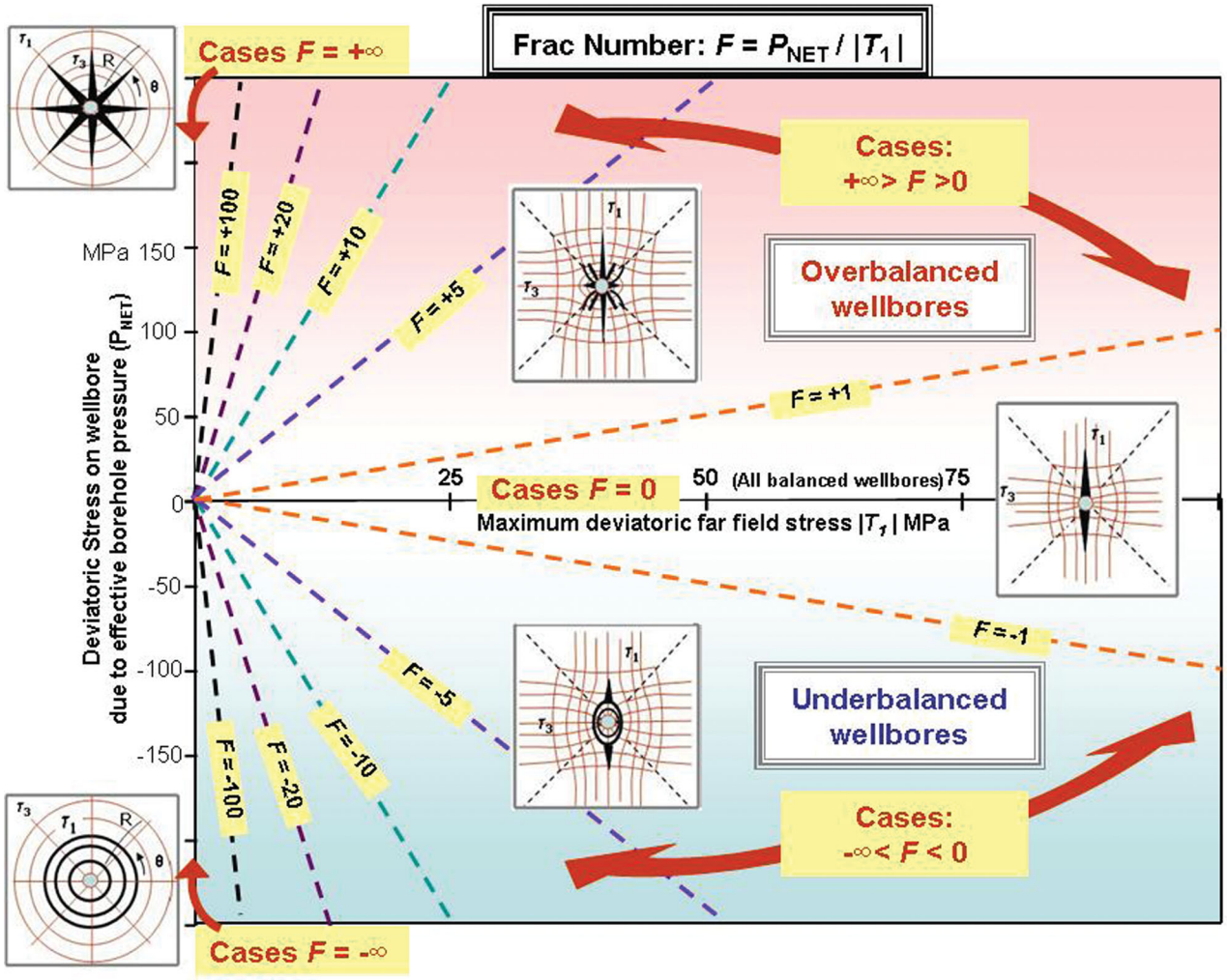

Figure 3. Stress trajectory pattern solutions for the full range of Frac numbers ($-\infty < F < +\infty$). Tension joints (black lines) in a vertical borehole are formed perpendicular to the extensional deviatoric stress, τ_3, and parallel to the τ_1 and τ_2 (out of plane). Vertical and horizontal plot axes are scaled differently to highlight sensitivity of the stress patterns for F values in the ranges $100 > F > 1$ and $-1 > F > -100$.

P_L and P_T. The pressure forces on the wellbore add up to $\vec{P}_{NET}$ in vector summation (Fig. 4).

If there is permeable contact between fluid in the drillhole (mud weight, P_M), and the formation fluid (P_F), any pressure changes inside the wellbore (by manipulation of P_M) will directly interact with the fluid pressure in the host rock (Fig. 5b). This results in a transient pressure gradient: formation fluid loaded by its overburden weight and by tectonic forces will excert a formation fluid pressure, which is then directly communicated to the mud pressure in wellbore. The mud pressure tends to rise or drop accordingly, but this takes time. If at the instant of first penetration by the drill bit a pressure diferential exists, it can be approximated by a static pressure differentials sketched in Fig. 5(a).

Underbalanced open drill hole completions ($\vec{P}_{NET} < 0$) have $|P_M| < |P_L + P_T + P_P|$, which is why $\vec{P}_{NET}$ will then always be negative (Fig. 4). Such cases will invariably have $F < 0$ (Figs 5a and b, lower cases) and stress trajectories in the lower part of Fig. 3 apply. In underbalanced wellbores, the net pressure $\vec{P}_{NET}$ is effectively a traction that pushes the wellbore surface inwards, and induces a tensional normal stress in the wellbore wall. That condition follows from the equilibrium equations that are accounted for in the stress function derivation of borehole stress in a previous analytical study (Weijermars 2011). Underbalanced well completions require a significant amount of specific equipment at the well site to ensure safe operations. Remember that in all commercial hydrocarbon reservoirs, the wellbore pressure is kept slightly lower than the average reservoir pressure—this is a prerequisite for a given amount of oil and gas in place to be recovered. During the process of well completion, there may be also brief intervals of time when the well is underbalanced, such as during underbalanced perforating operations.

For balanced well completions ($\vec{P}_{NET} = 0$), P_M is engineered with mud loads to aim for $\vec{P}_{NET}$ close to zero at most depths (Figs 5a and b, middle cases). However, P_F is highly variable in natural rocks (Dugan & Flemings 2000), and may be difficult to balance at each specific level and therefore $\vec{P}_{NET} = 0$ is a rare condition. Wellbores are commonly engineered to be overbalanced during the construction process by selecting the mud weight such as to provide a positive $\vec{P}_{NET}$ at all points in the open hole. The minimum mud weight gradient is therefore limited by the highest formation pressure (P_F) and all of the rest of the formations crossed by the wellbore will then experience a significant overbalance. This is primarily a well control (safety) issue. The hydrostatic pressure of the wellbore fluid is the 'primary barrier'

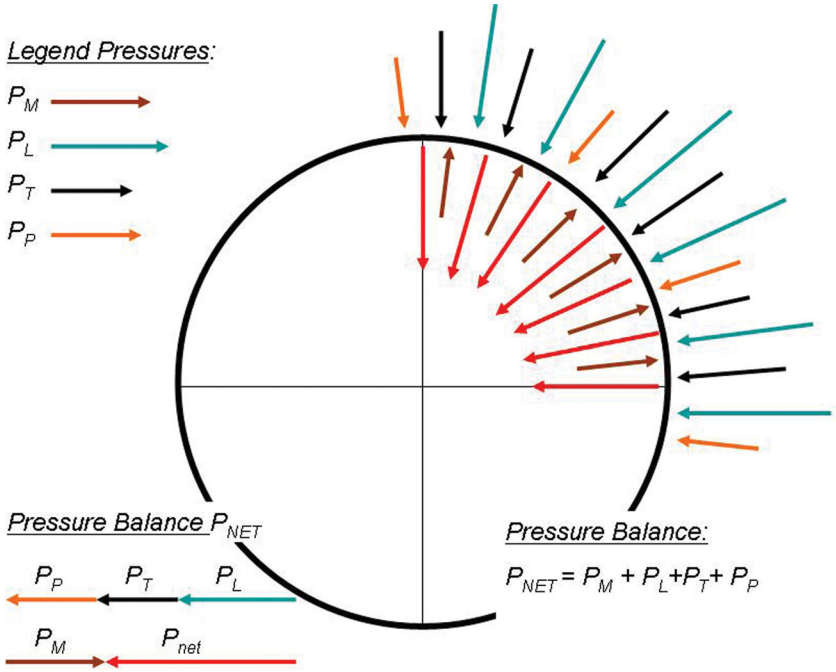

Figure 4. Pressure components on wellbore result in $\vec{P}_{\mathrm{NET}}$, which is an effective, deviatoric stress on the wellbore surface. $\vec{P}_{\mathrm{NET}}$ traction units are positive when the effective stress is pointing outward, negative when it points inwards.

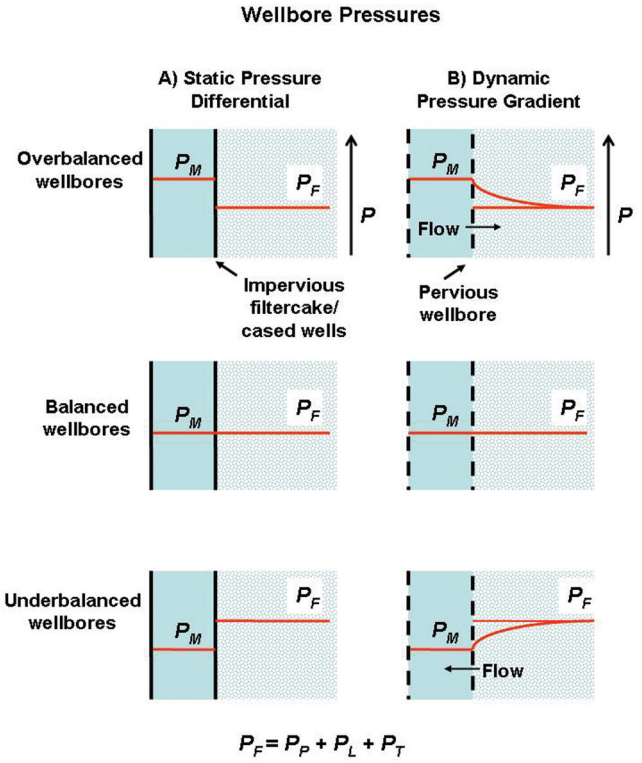

Figure 5. Wellbore pressure profiles for (a) static and (b) transient cases. Static situations apply to the first instant of formation penetration by the drill bit and will be maintained when a filter-cake screens out the pore space. This situation also applies to tight formations that cannot effectively communicate pore pressure with wellbore fluid and cased wells. The red lines show the pressure distribution. The borehole fluid pressure is denoted by P_{M} and formation pressure by P_{F} (see text).

between the formations fluids (potentially hydrocarbons) and the surface.

For the overbalanced sections ($\vec{P}_{\mathrm{NET}} > 0$) of the wellbore, $\vec{P}_{\mathrm{NET}}$ will push the wellbore surface outwards (Figs 5a and b, upper cases) and thereby exerts a compressional normal stress on the wellbore wall and the stress trajectories in the upper half of Fig. 3 apply. The response of the host rock is elastic distortion, until failure is initiated (Fossen 2007). When the critical tensile strength, σ_{c}, is reached by the principal stress, oriented as outlined by the trajectory pattern near the wellbore, hydraulic tensile fractures will open.

6 FRAC NUMBER VARIATIONS

Although most wellbores in the industry intend to be drilled as overbalanced wellbores, unanticipated high formation pressures remain a drilling hazard. That is why great care is taken to avoid taking a kick, and drilling equipment is designed to avoid sudden well pressure drops in order to reduce wellbore instability.

From a theoretical viewpoint, negative F numbers may arise at specific intervals along the full length of a wellbore not only during underbalanced open-hole drilling but also at specific depths where overpressured formations occur. Such overpressured formations, if connected to an underbalanced wellbore, will result in $\vec{P}_{\mathrm{NET}} \ll 0$ (Figs 6a–d), and can be characterized by negative Frac numbers. Underbalanced boreholes will have negative F values even in the absence of any far-field stress ($T_1 \geq 0$). Very large negative F numbers ($F \rightarrow -\infty$) may occur when there is negligible far-field stress ($\tau_1 \sim 0$) and P_{NET} is negative (and when $\left|\vec{P}_{\mathrm{NET}}\right| \gg |\tau_1|$). For example, consider a vertical wellbore and vary the net pressure on the wellbore to range between $-\infty < \vec{P}_{\mathrm{NET}} \ll 0$. The stress trajectory pattern for these cases always resemble the spider-web stress trajectory solution (Fig. 7a), which confines the near wellbore tension fractures to circumferential surfaces in concentric zones.

For the sake of completeness, when the F number become positive, the directions of τ_1 and τ_3 (largest and smallest principal

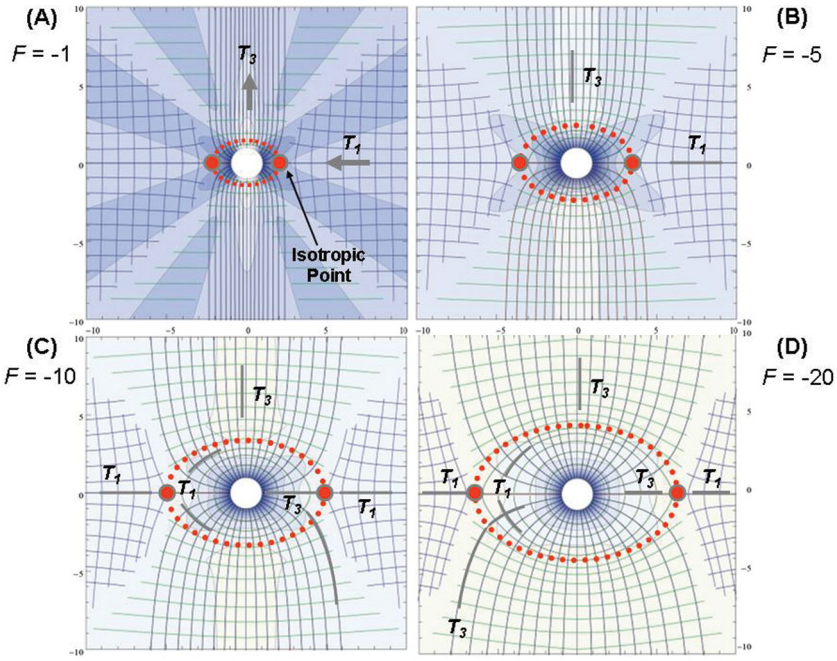

Figure 6. (a–d) Stress trajectory patterns around underbalanced wellbores. The wellbore pressure is lower than the formation pressure ($\overrightarrow{P}_{\rm NET} < 0$). The F number (ratio of $\overrightarrow{P}_{\rm NET}$ and far field stress) is negative for all wellbores shown. Colour fringes are for τ_3 normalized by $\overrightarrow{P}_{\rm NET}$ and isobar contour interval is 0.25 for (a) and 0.1 for (b–d). Red dots are neutral or isotropic points and dotted ellipse gives the fracture cage outline. Note that tension stress inside the fracture cage is consistently oriented in the radial direction.

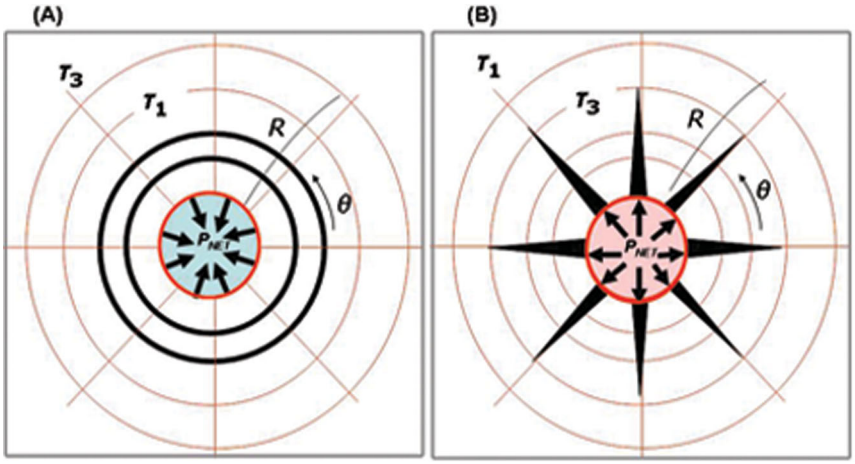

Figure 7. (a) Negative Frac numbers F nearing $-\infty$ give spider web stress trajectory patterns and occur around underbalanced boreholes ($\overrightarrow{P}_{\rm NET} \ll 0$). The direction of preferred tensional failure (solid black circles) is parallel to the τ_1 trajectories, normal to the least principal stress τ_3. (b) Large positive Frac numbers F nearing $+\infty$ are typical for overbalanced boreholes ($\overrightarrow{P}_{\rm NET} \gg 0$). Stress trajectory patterns also resemble a spider web pattern, but the direction of preferred tensional failure (black spikes) is now radial due to a reversal of the principal stresses. In practice, bi-winged tension fractures may prevail due to the stress cage effect.

stresses) interchange for a positive $\overrightarrow{P}_{\rm NET}$ in overbalanced wellbores, and tension fractures will tend to open in the radial planes (Fig. 7b). The intermediate cases for positive F number conditions ($0 < F < +\infty$) are illustrated in Figs 8(a)–(d), with pressure isobars colour coded. These stress trajectory patterns occur for $\overrightarrow{P}_{\rm NET} > 0$, which applies to underpressured formations connected to overbalanced wellbores (Figs 8a–d).

7 FRACTURE CAGES

A completely new insight emerges from our analysis of the full range of negative Frac numbers ($-\infty < F < 0$). Figs 6(a)–(d) summarize the stress trajectories for negative F values. What is relevant is that a central region occurs around the wellbore where τ_1 trajectories form closed ellipses. These trajectories preclude any fracture initiated at the wellbore to escape outwards from the elliptical area. Fractures may only propagate along the τ_1 trajectories because tensile fractures always form perpendicular to the tensile stress (τ_3) allowing dilation and opening in the direction of τ_3. The fracture cage outlines the region occupied by the elliptical τ_1 trajectories and is an ellipse that intersects the two neutral points of isotropic stress (Figs 6a-d).

It is important to realize that the horizontal line through the two neutral points connects zones of principal stress reversal, that is,

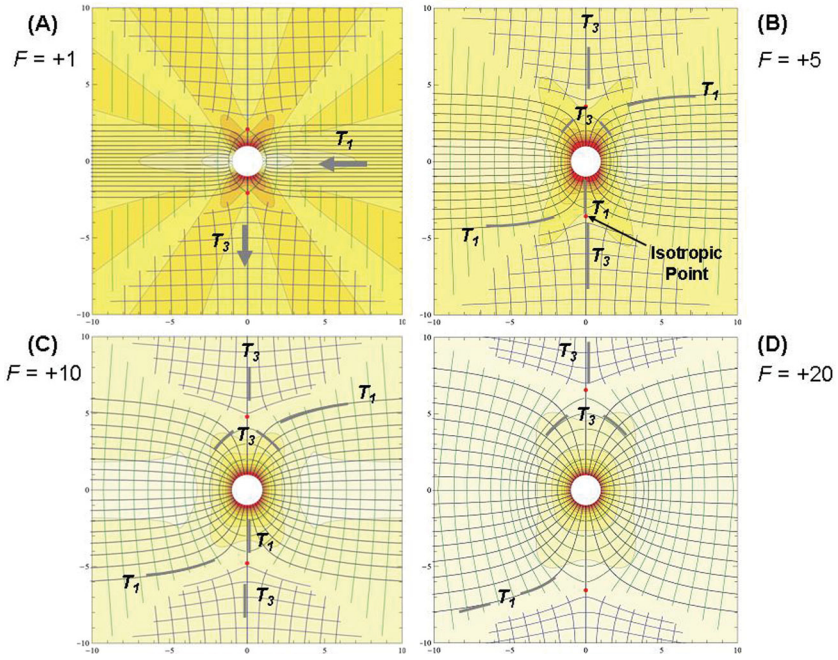

Figure 8. (a)–(d) Stress trajectory patterns around overbalanced wellbores. Formation pressure is lower than the wellbore pressure ($\overrightarrow{P}_{\rm NET} > 0$). The ratio of $\overrightarrow{P}_{\rm NET}$ and far field stress is positive ($F > 0$) for all cases shown. Colour fringes are for τ_1 normalized by $\overrightarrow{P}_{\rm NET}$ and contour interval is 0.25 for (a) and 0.1 for (b)–(d). Red dots are neutral points. Note that compression stresses are in the radial directions near the wellbore.

with a change in the deviatoric stress sign. The compressional stress τ_1 due to the far field stress will be deflected inside the fracture cage zone (Figs 6c and d). A tensional stress τ_3 on the horizontal line inside the fracture cage is aligned with the compressional stress τ_1 outside the fracture cage zone. These two principal stresses are separated by the neutral points where their respective magnitudes are reduced to zero.

The equation for the fracture cage ellipse, in polar coordinates with the origin at the centre of the ellipse, is given by (Fig. 9a):

$$R(\theta) = (E_{\rm L}E_{\rm S})\big/[(E_{\rm L}\sin\theta)^2 + (E_{\rm S}\cos\theta)^2]^{1/2} = 0. \qquad (9)$$

The long axis of the ellipse, $E_{\rm L}$, follows from the isotropic (or neutral) point condition, $\tau_{\rm r} = \tau_\theta$ at $\theta = 0$, where the shear stress $\tau_{{\rm R}\theta}$ vanishes, which gives the relationship between F and $E_{\rm L}$,

$$E_{\rm L}^4 + (2F - 3)E_{\rm L}^2 + 3 = 0. \qquad (10)$$

Normalizing the ellipse axis $E_{\rm L}$ by the borehole radius, a, gives the non-dimensional distance $E_{\rm L}^*$ ($= E_{\rm L}/a$), measured from borehole centre to the neutral point. Solving eq. (9) for F in the quadratic formula gives the non-dimensional long axis, $E_{\rm L}^*$, of the fracture cage ellipse:

$$E_{\rm L}^* = {\rm sqrt}\left\{\left[-2F + 3 + {\rm sqrt}\left(4F^2 - 12F - 3\right)\right]/2\right\}, \quad \text{for } F < -0.45. \qquad (11)$$

This equation also shows that the fracture cage area grows when the magnitude of $|\overrightarrow{P}_{\rm NET}|$ increases over τ_1. The non-dimensional short axis, $E_{\rm S}^*$, of the stress cage ellipse follows from $E_{\rm S}^* = E_{\rm S}/a$. Accurate dimensions for the fracture cage based on the Frac number are given by expression (11) and plotted in Fig. 9b.

8 DYNAMIC SOLUTIONS

Hydraulic fracture growth from a wellbore under plane strain conditions has been modelled in earlier numerical studies (Zhang *et al.* 2011a,b), using a displacement discontinuity boundary element method. The dynamic approach complements the above static analysis. A fully coupled hydraulic fracture model can analyse problems involving a Newtonian fluid injected at constant rate to grow a hydrofrac in impermeable rock. The fracture surface contact and frictional sliding are accounted for by a history dependent Coulomb friction law criterion. The numerical code ensures dynamic coupling of the fracture growth and the hydraulically induced stress around the borehole. For more detailed descriptions of the model assumptions readers are referred to earlier studies (Zhang *et al.* 2009, 2011a,b; Jeffrey & Zhang 2010).

The static analytical solutions for the fracture cage (Figs 6a–d) are compared here to dynamic numerical solutions. Figs 10(a)–(c) show the numerical model for a case where an incipient fracture at the wellbore is respectively shorter and longer than the distance to the fracture cage rim. This is for an open-hole completion which is modelled by assuming no mud fluid pressure applied on the wellbore surface. Alternatively, think of a wellbore effectively shielded from hydraulic pressure by the presence of a steel casing. The hydraulic fluid is injected from slotted source located where the initial crack meets the wellbore. The short fracture stays trapped in the fracture cage when hydraulically loaded (Figs 10a–c). The longer fracture extends long enough to have its fracture tip outside the fracture cage propagating further outwards into the rock matrix to align with the far field τ_1 trajectories (Figs 10a–c). Fig. 10(d) shows the analytical and numerical cases side by side for similar conditions, which confirms the validity of the numerical results; the fracture cage sizes match perfectly. The analytical stress trajectory solution explains why the short frac curls around the wellbore and the long frac propagates towards the far field stress axis.

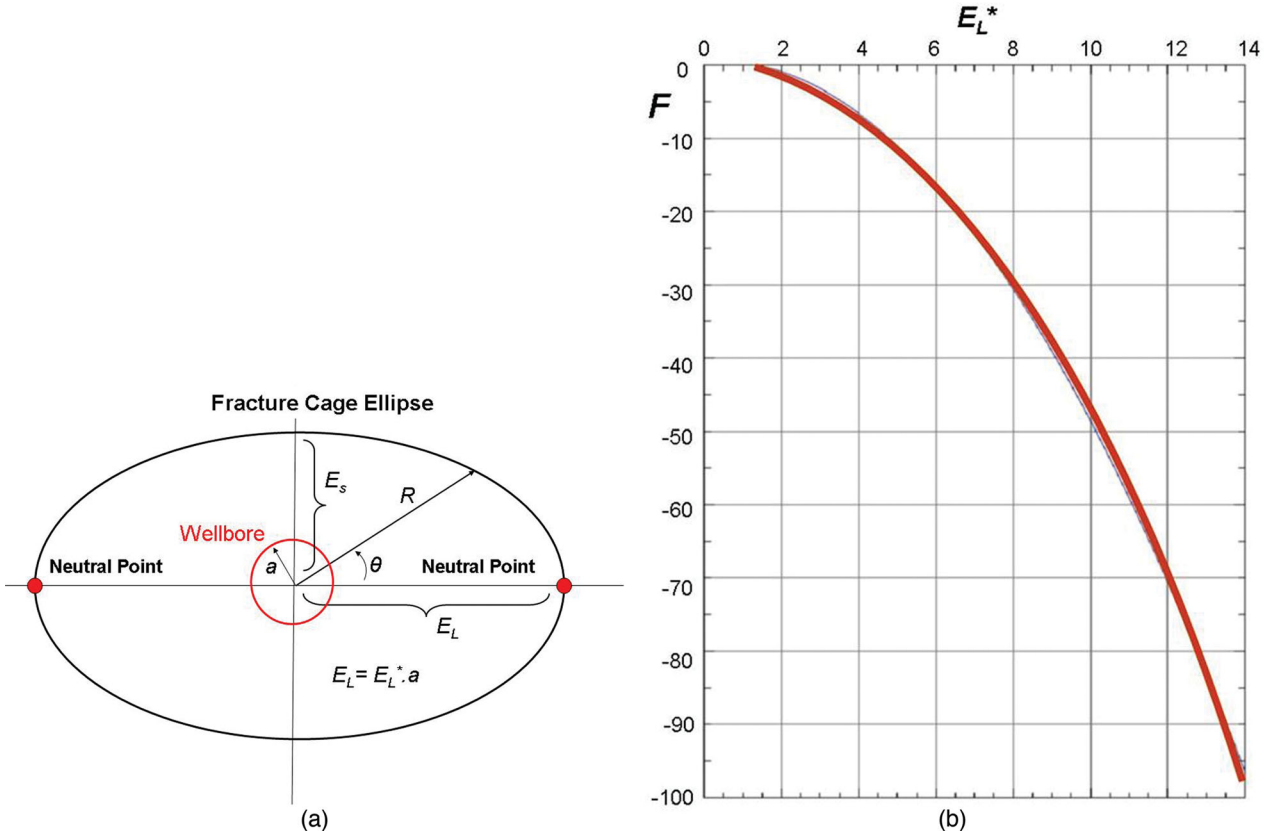

Figure 9. (a) Polar coordinates for stress cage ellipse around wellbore. Red dots are the neutral points where no deviatoric stress exists ($\tau_1 = \tau_3 = 0$). (b) Dimension of the fracture cage longest ellipse axis E_L^* ($= E_L/a$), as a function of the Frac number F (based on eq. 11).

The dimensional stress field used is determined by $\sigma_1 = 80$ and $\sigma_3 = 40.1$ MPa. As the Poisson ratio is 0.25, the out-of-plane stress is $0.25 \times (80–40) = 30$ MPa. This implies $\overrightarrow{P}_{NET} = -P_T = -(\sigma_1 + \sigma_2 + \sigma_3)/3 = -50$ MPa and $\tau_1 = \sigma_1 - P_T = 30$ MPa; the Frac number is thus given by $F = \overrightarrow{P}_{NET}/|\tau_1| = -1.66$. The distance to the fracture cage rim for this Frac number is analytically predicted by eq. (11), and for $F = -1.66$ the distance $E_L^* = 2$. Remember the dimensional distance $E_L = 2 \times a$, with 'a' the dimensional borehole radius.

Negative Frac numbers occur when $\overrightarrow{P}_{NET}$ is negative and $|\overrightarrow{P}_{NET}|$ increases relative to $|\tau_1|$, so that $-\infty < F < 0$. For example, if the two principal total stresses in the numerical analysis of Figs 10(a)–(c) are set at 95 and 85 MPa, and static pressure component $P_T = 75$ MPa $= -\overrightarrow{P}_{NET}$ and $\tau_1 = 20$ MPa, then $F = -3.75$ and the distance to the neutral point increases to $E_L^* = 3.2$. The fracture cage region will be wider or narrower depending on the relative magnitude of any negative $\overrightarrow{P}_{NET}$ on the wellbore as factored into the F number (Fig. 9b). The axial length E_L^* of the fracture cage increases when negative Frac numbers grow from $0 \geq -\infty$. The preferred direction of tension fracturing is always parallel to τ_1 trajectories when the critical stress for tension failure is reached.

9 PRACTICAL IMPLICATIONS

Our theoretical descriptions of the occurrence of fracture cages holds practical implications (1) for the control of potential fracture caging (see Box 1) effects in formations with highly variable pressures during regular drilling operations (vertical, horizontal, directional) and (2) for the design of sophisticated engineering solutions for hydraulic fracture placement. These implications are briefly highlighted below.

9.1 Regular drilling operations

Well pressure control is a main concern in drilling operations, which is why well testing and special equipment are key for successful well completions. In spite of all precautions, unusual high formation pressures may still occur, which is why blowout preventers are mounted on the wellbore. Although well blowout is well known to be due to overpressured formations, the Frac number provides a parametric tool to monitor the risk of fracture caging at any specific depth.

Balancing the formation pressure of a leading section along the wellbore is still critically dependent on leak-off tests, which provide a measure for the static bottom hole pressure (BHP; and is affected by the average formation pressures along the entire section of open-hole wellbores). BHP may provide an estimate of P_F at the depth of a particular target formation and can be combined with regular mud pressure gradients to obtain estimates for $\overrightarrow{P}_{NET}$. Formation pressures can also be inferred from log data. The leak-off pressure (or shut-in BHP) is commonly higher than the flowing BHP (FBHP) obtained via wireline BHP gauges (Lin *et al.* 2008), which is in accordance with our model of transient or dynamic pressure gradients (Fig. 5b).

Fig. 11 illustrates the fracture caging effect that may occur during drilling when a particular formation pressure remains unintentionally underbalanced by the wellbore fluid pressure. The borehole will enlarge for negative Frac numbers in combination with

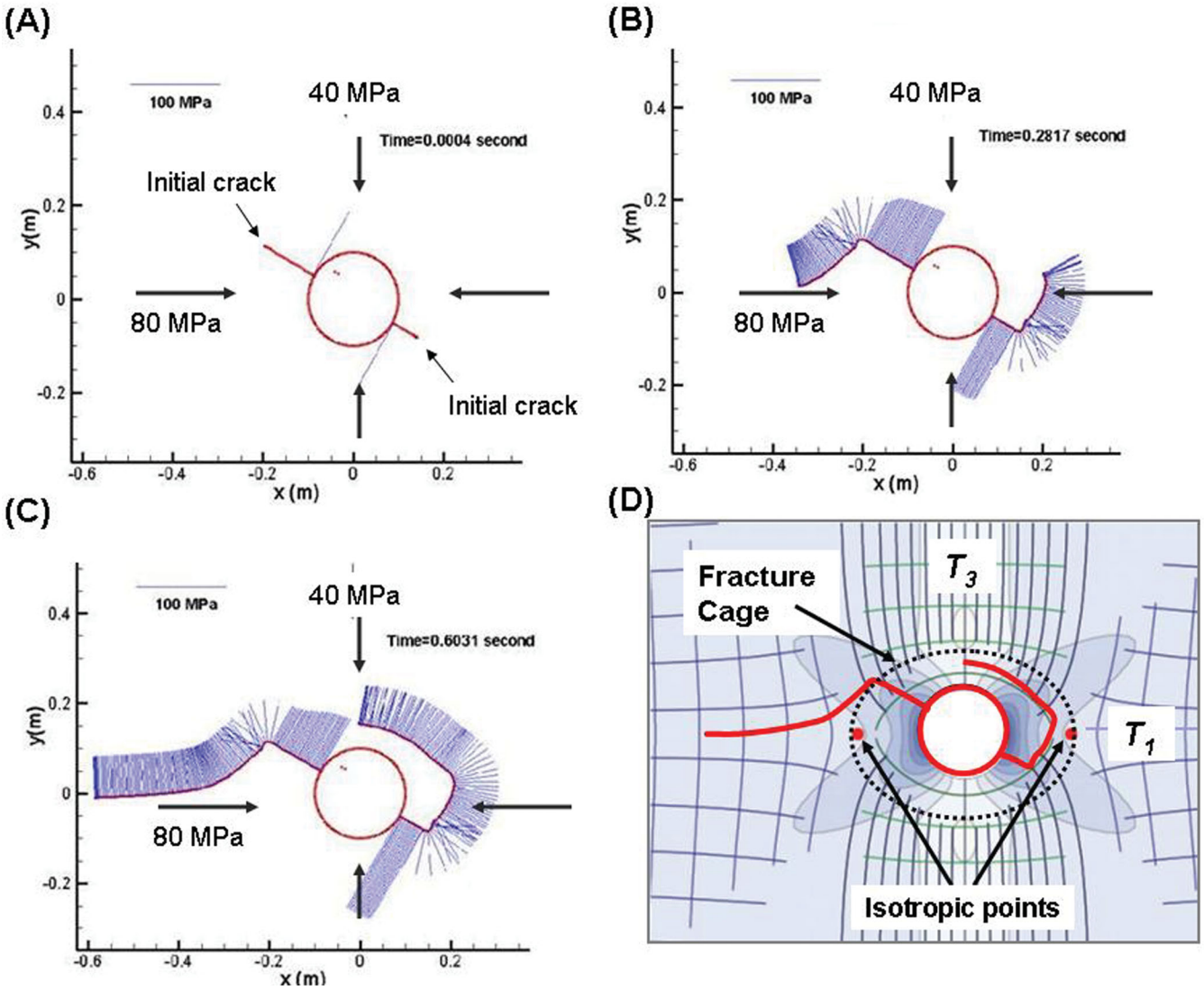

Figure 10. (a)–(c) Numerical simulation with initial cracks near the wellbore, one too short (0.64 times borehole radius, right fracture) and the other long enough (1.28 times borehole radius, left fracture) to escape outwards from the fracture cage ($F = -1.66$). The in-plane total far field stresses are specified as 40 and 80 MPa, respectively. Wellbore pressure is zero, but the pressure along the hydraulic fracture is not zero and intensity is given by the scaled blue lines. Material parameters for this simulation are: $E = 30$ GPa, Poisson ratio $= 0.25$, KIC (Toughness) $= 5.62$ MPa m$^{-1/2}$ (to slow down crack growth), dynamic viscosity $= 0.01$ Pas, and initial hydraulic injection rate $= 0.0004$ m^2 s^{-1}, fracture friction coefficient $= 0.5$. Time steps are for (a) 0, (b) 0.3 and (c) 0.6 s after hydraulic injection. (d) Analytical stress trajectory solution for $F = -1.66$ delineating the fracture cage formed by the τ_1 stress ellipse around the wellbore. Isobar contour interval is 0.3 ($\tau_3/\vec{P}_{\mathrm{NET}}$).

absolute stress levels exceeding the criteria for tensional failure and shear breakout. The borehole may continue to grow larger by 'fracture caging' in runaway mode when the borehole has penetrated the anomalously high and unanticipated overpressured formation (Figs 6a–d, 7a, 10a–d). Concentric or elliptical fractures will form and the diameter of the hole will 'spontaneously' enlarge due to concentric caving. Caved rock fragments mix into the drilling mud and transport to the surface with the upwelling of expelled formation fluid. Rock fragments and drilling fluid will continue to move upwards until the formation pressure drops enough (and renders the Frac number positive) to arrest the upward flow of liquids and caving fragments.

Fig. 12 is a controlled laboratory experiment using confining pressure only, which leads to borehole collapse when the induced stresses near the wellbore become supercritical. In contrast, formations with overbalanced wellbores will not provide any 'fracture caging' risk during drilling operations. Concentric fractures (Fig. 7a) cannot form and radial fractures will form instead (Fig. 7b). Formations penetrated by overbalanced wellbores tend to attract—rather than expulse—borehole fluid. Borehole integrity is not at stake, but accelerated scaling of particles in a filter cake on the wellbore may prevent fluid exchange through the wellbore wall and may lower well productivity even after well clean-up when the wellbore is prepared to become a conduit for hydrocarbon production.

9.2 Hydraulic fracturing

Our study holds implications for the planning of hydrofrac jobs in optimum synergy with the geomechanics and ambient stress conditions of the target zone. Assume a tight hydrocarbon

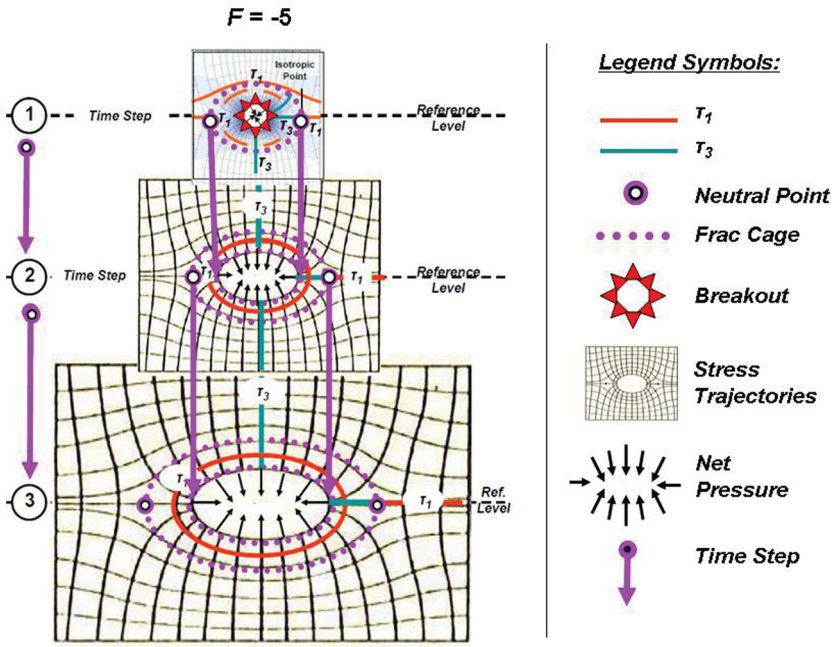

Figure 11. Well failure sequence (time steps 1, 2 and 3) in fracture caging runaway mode. The runaway process will only halt when the borehole pressure becomes balanced again, either by formation pressure decline due to blowout or by regaining well-pressure control (preferably before the blowout occurs).

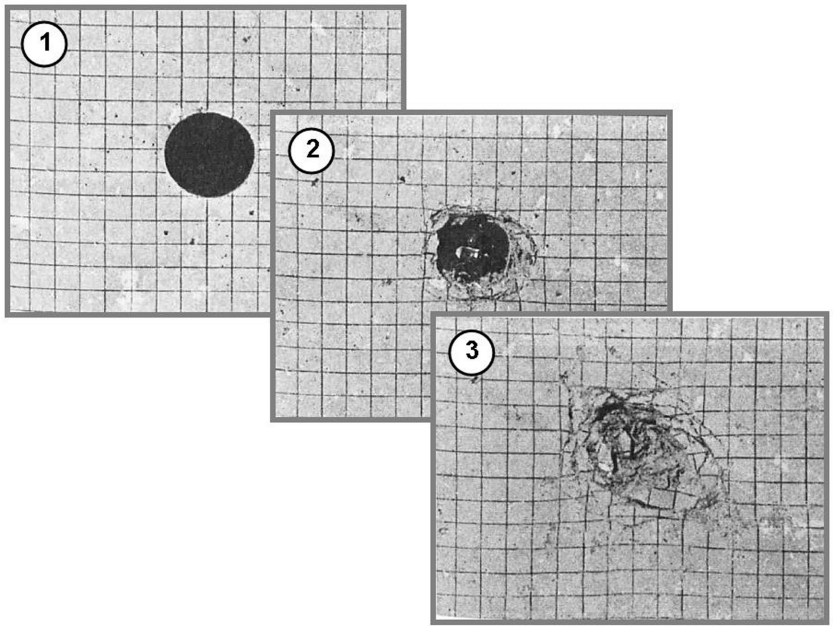

Figure 12. Well failure sequence (time steps 1, 2 and 3) in concrete block ($30 \times 30 \times 30$ cm^3) subjected to confining pressures of (1) 0 MPa, (2) 23.8 MPa and (3) 24.5 MPa (after TU Delft laboratory tests by Roest *et al.* (1989)).

formation with relatively few natural fractures. Completion efforts in such unconventional reservoirs must place hydraulic fractures to stimulate well performance. Sweet spots in unconventional oil and gas plays are the outcome of effectively locating rock volumes with favourable hydrocarbon maturity, combined with petrophysic and geomechanic properties that can be optimally accessed using cost-effective well architecture and stimulation techniques (King 2010).

A wellbore penetrating a pristine, unfractured section of the reservoir rock should be oriented such that the frac architecture results in optimum well productivity. Knowing the geometry of the fracture region envelope helps to optimize the well productivity/cost ratio. This means the wellbore orientation and wellbore hydraulic net pressure should be engineered to control, manipulate and exploit Frac numbers near the wellbore such that hydraulic tension fracs and shear faults improve the well productivity. Economic production requires selective placement of stages in the production plan and exclusion of low-productivity sections along the wellbore. Our Frac number provides a new tool to attempt precision engineering of hydraulic fractures.

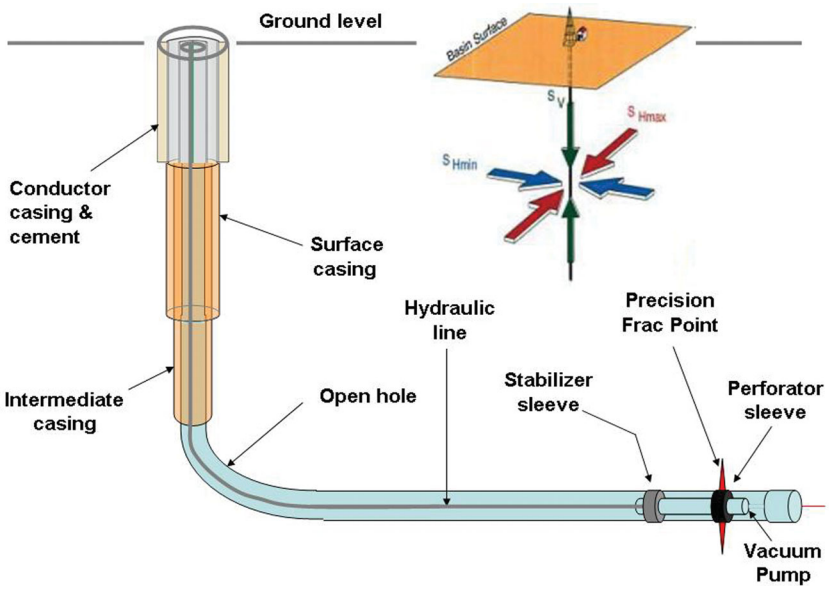

Figure 13. Innovative well completion method using a hydraulic fracturing tool, which comprises an expandable perf-and-frac sleeve that puts the hydraulic nozzles firmly onto the open-hole wellbore. Vacuum pump at the tool's leading edge is employed to 'suck' the tool towards the borehole toe before the perf-and-frac operation starts.

This process can be further optimized by introducing a precision fracking tool. Fig. 13 shows the principle design of such a hydraulic fracturing tool that allows separate control of Fracking pressure and wellbore pressure, which is critical for controlling the magnitude of F number. The design suggested here is for an open-hole completion and the annulus of mud or drilling fluid controls the well pressure. Well completion typically involves carefully positioned casings (conductor, surface and intermediate casings) until the production zone is reached. Between the various steel casing sections cement is commonly used to seal off the wellbore (Baker 1983). The cement filled spaces between casing strings and any packers in the annulus (between the production liner and the casing) act as pressure barriers. Gas migration in the annulus between casing and wellbore may lead to gas-flow channels in cement and can compromise completion integrity and wellbore safety. The unwanted gas flow can be mitigated using inflatable or swellable elastomers as annular packers between the casings (Gary 2011).

The frac tool is comprised of a separate perforator gun section with its own hydraulic line and can be emplaced by the annulus pressure or moved in position with commercially available down-hole tractor wheels. The expandable perforator gun sleeve is used to put the hydraulic nozzles firmly onto the wellbore. It is then possible to perf-and-frac progressive sections of the wellbore, working from the toe towards the heel of the well. The advantage of this precision frac tool design is a better control of the induced Frac number, using the fluid pressure in the annulus of the open hole to control the Frac number while the nozzles inject hydraulic fluid into the formation. The precision frac tool must perforate deep enough with injection rates set up to preferentially open up radial tension fractures, microcracks and faults to emplace proppants that can keep frac conduits open for hydrocarbon migration. The stabilizer sleeve is an inflatable packer that contains tubes in order not to seal off the annulus and instead allows for a dual injection frac modulation as described by Daneshy (2011). The nozzles in the precision frac tool's perf-and-frac sleeve, at the leading edge of the tool (Fig. 13), can be engineered to control the frac initiation point within the open-hole interval. The initial perforation by guns or charges must penetrate into the wellbore wall rock to create a conduit for the hydraulic fluid to ensure no fracture caging will occur. Once the formation is ready for production, a production liner of smaller diameter may be placed inside the producing stages all the way up to the surface.

10 CONCLUSIONS

Controlled well engineering requires detailed modelling of the stress trajectories around the wellbore as demonstrated here. Our study introduced a number of new terms, which are concisely defined and summarized in Box 1. The propagation direction of fractures originating from the wellbore can be theoretically predicted by the Frac number, which controls the stress trajectory patterns near the wellbore. Well control critically depends on measurements of the far field principal deviatoric stress, τ_1, and the manipulation of the wellbore net pressure ($\overrightarrow{P}_{NET}$) at all depths. The Frac number provides a concise parameter to help monitor well stresses, and improve safety by pinpointing the conditions that may lead to the occurrence of borehole fracture caging. Numerical modelling has confirmed that fractures shorter than the fracture cage dimensions cannot propagate out of the fracture cage and enhance the fracture caging effect. This knowledge is also useful to improve the effectiveness of hydraulic fracture stimulation for oil and gas recovery from tight formations.

Our results further suggest that the Frac number, as a monitoring tool, should be embedded in driller's monitoring software packages. Our study describes the fracture caging mechanism, which must be taken into account in drilling operations and engineered with purpose or avoided when hazardous. The maintenance of wellbore control when drilling with underbalanced pressures remains extremely important for ensuring wellbore integrity and safe well completions. Because of the larger formation pressure involved, deep boreholes run tremendous risk if the Frac number is not monitored with a keen eye for the avoidance of fracture caging. If fracture caging runaway (see Box 1) is triggered, it may be hard to stop. Setting alarm bells

more precise than today, by utilizing the Frac number, provides an additional safety layer.

We hope the insights provided in our study will help to make drilling safer and more accurate. Future drilling efficiency could be improved by utilizing the fracture caging effect in a controlled way to enlarge wellbores while using smaller drill bits. There may also be scope for sleeker fracking tools (Fig. 13). The Frac number creates new possibilities for precision fracking that aims to control fracture patterns by manipulating the net pressure in the nominator of the Frac number under a given tectonic stress regime. Today's hydraulic fractures are created using a combination of explosives and hydraulic pressures. Our approach advocates using these energy sources with more subtleness (i.e. with figure-skating elegance versus today's brutely powered speed skating), utilizing the natural stress directions where possible and actively manipulating the near wellbore stress field using the proposed precision fracking device. Effective stimulation by hydraulic fracturing of shales and tight sands for the extraction of hydrocarbon resources remains a topic of global importance. The Frac number opens up new avenues for safer drilling and improved fracking techniques.

ACKNOWLEDGEMENTS

This manuscript benefited from numerous discussions and additional comments during multiple iterations in the peer review process. Fruitful discussions with Karl-Heinz Wolf at TU Delft and the Drilling Awareness Group at Shell are gratefully acknowledged. Xi Zhang acknowledges fruitful discussions with CSIRO colleagues Rob Jeffrey and Andy Bunger. Ruud Weijermars has been generously seconded by Alboran Energy Strategy Consultants to spend time on well mechanics research.

REFERENCES

Ahmed, T. & Meehan, N., 2012. *Advanced Reservoir Management and Engineering,* 2nd edn, Gulf Publishing, Houston.

Alberty, M.W. & McLean, M.R., 2004. A Physical Model for Stress Cages. *SPE Annual Technical Conference and Exhibition,* Houston, Texas, USA, 2004 September 26–29. SPE90493.

Baker, R., 1983. *Oil & Gas—the Production story—a PETEX Primer. Petroleum Extension Service Division of Continuing Education,* University of Texas at Austin, Texas.

Daneshy, A., 2011. Dual-injection frac systems in horizontal wells, *World Oil,* **232**(12), 55–57.

Dugan, B. & Flemings, P.B., 2000. Overpressure and fluid flow in the New Jersey Continental Slope: implications for slope failure and cold seeps, *Science,* **289,** 288–291.

Durrheim, R.J., Jager, A.J., Klokow, J.W. & Booyens, D., 1995. Back analysis to determine the mechanism and risk of rockbursts—3 case histories from South African gold mines, in *Proceedings of the 26th International Conference of Safety in Mines Research Institutes,* Vol. 5, pp. 41–56, Central Mining Institute, Katowice, Poland.

Fossen, H., 2010. *Structural Geology,* Cambridge University Press, Cambridge.

Gary, D.A., 2011. Using casing annular packers to prevent shallow gas migration to surface in shale wells, *World Oil,* **232**(12), 43–45.

Jeffrey, R.G. & Zhang, X., 2010. Mechanics of hydraulic fracture growth from a borehole, SPE 137393, in *Proceedings of the Canadian Unconventional Resources and International Petroleum Conference,* Calgary, Alberta, Canada, 2010 October 19–21.

King, G.E., 2010. Thirty years of gas shale fracturing. What have we learned? SPE 1334567.

Kirsch, G., 1898. Die Theorie der Elastizität und die Bedürfnisse der Festigkeitslehre, *Zeitschrift des Vereines deutscher Ingenieure,* **42**(28), 797–807.

Lin, W., Yamamoto, K., Ito, H., Masago, H. & Kanamura, Y., 2008. Etsimation of minimum principal stress from an extended leak-off test on board the Chikuyi drilling vessel and suggestions for fracture test procedures, *Scientific Drilling,* **6,** 43–47.

Malvern, L.E., 1969. *Introduction to the Mechanics of a Continuous Medium,* Prentice-Hall, Englewood Cliffs, New Jersey.

Ortlepp, W.D., 2001. The Mechanism of a Rock Outburst in a Quartzite Tunnel in a Deep Gold Mine. Rockbursts and Seismicity in Mines-*RaSiM5, South African Institute of Mining and Metallurgy*, South Africa, p. 53–58.

Roest, J.P.A., Kamp, W., Zhongjie, H. & Cockram, M.J., 1989. Basic research for the de-stressing of the rock ring surrounding a gallery under severe stress, in *Proceeding of the International Society for Rock Mechanics International Symposium,* 1989 August 30–September 2, A.A. Balkema, Dordrecht, Pau, France.

Tovar, J. & Bhat, S., 2011. Characterization of stress caging effect for resolving wellbore integrity probems in fractured formations—experimental results, VII INGEPET 2011 (EXPL-2-JT-02).

Vardoukalis, I., Sulem, J. & Guenot, A., 1988. Borehole instabilities as bifurcation phenomena, *Int. J. Rock Mech. Min. Sci. Geomech., Abstr.,* **25**(3), 159–170.

Wang, M.H., Soliman, M.Y. & Towler, B.F., 2008. *Investigation of Factors for Strengthening a Welllbore by Propping. 2008 IADC/SPE Drilling Conference,* Orlando, Florida, USA, 2008 March 4–6. IADC/SPE 112629.

Weijermars, R., 1993. Estimation of palaeostress orientation within deformation zone between two mobile plates, *Geol. Soc. Am. Bull.,* **105**(1), 491–1510.

Weijermars, R., 1998. *Principles of Rock Mechanics,* Alboran Science Publishing, Amsterdam, Now available as open courseware at http://ocw.tudelft.nl/courses/applied-earth-sciences/principles-of-rock-mechanics/readings/.

Weijermars, R., 2011. Analytical Stress Functions applied to Hydraulic Fracturing: Scaling the Interaction of Tectonic Stress and Unbalanced Borehole Pressures. American Rock Mechanics Association, ARMA 11–598, in *Proceedings of the 45th US Rock Mechanics/Geomechanics Symposium,* Francisco, CA, 2011 June 26–29.

Weijermars, R. & Schulz-Ela, D., 2012. Visualizing stress trajectories around pressurized wellbores. *SPE 152559. SPE/ EAGE European Unconventional Resources Conference and Exhibition,* Vienna, Austria, 2012 March 20–22.

Weijermars, R., Zhang, X. & Schultz-Ela, D., 2012. Unrecognized 'fracture caging' could make shale gas drilling projects safer and more profitable, *First Break,* **30**(2), 35–36.

Zang, A. & Stephansson, O., 2009. *Stress Field of the Earth's Crust,* Springer, Londen.

Zhang, X., Jeffrey, R.G. & Thiercelin, M., 2009. Mechanics of fluid-driven fracture growth in naturally fractured reservoirs with simple network geometries, *J. geophys. Res.-Solid Earth,* **114,** B12406.

Zhang, X., Jeffrey, R.G. & Bunger, A.P., 2011a. Hydraulic fracture growth from a non-circular wellbore. American Rock Mechanics Association, ARMA 11–333, in *Proceedings of the 45th US Rock Mechanics/Geomechanics Symposium,* San Francisco, CA, 2011 June 26–29.

Zhang, X., Jeffrey, R.G., Bunger, A.P. & Thiercelin, M., 2011b. Initiation and growth of a hydraulic fracture from a circular wellbore, *Int. J. Rock Mech. Min. Sci.,* **48,** 984–995.

Zoback, M., 2007. *Reservoir Geomechanics,* Cambridge University Press, Cambridge.

SUPPORTING INFORMATION

Additional Supporting Information may be found in the online version of this article:

Movie S1. Movie of propagation of short initial crack inside a fracture cage with conditions as specified in Fig. 10 of this article.

Movie S2. Movie of propagation of longer initial crack crossing the fracture cage zone with conditions as specified in Fig. 10 of this article.

Movie S3. Movie with both a long and a short initial crack propagating simultaneously; the short one trapped inside the fracture cage, the longer one escaping outwards to align with the direction of the maximum principal stress as in Fig. 10(d) (http://gji.oxfordjournals.org//lookup/supp1/doi:10.1093/gji/ggt060/-/DC1).

Please note: Oxford University Press are not responsible for the content or functionality of any supporting materials supplied by the authors. Any queries (other than missing material) should be directed to the corresponding author for the article.